

Spatially engineered polarization states and optical vortices in uniaxial crystals

Tatyana A. Fadeyeva¹, Vladlen G. Shvedov^{1,2,3}, Yana V. Izdebskaya²,
Alexander V. Volyar^{1,*}, Etienne Brasselet⁴, Dragomir N. Neshev²,
Anton S. Desyatnikov², Wieslaw Krolikowski³, and Yuri S. Kivshar²

¹Department of Physics, Taurida National University, Simferopol, Crimea, Ukraine,

²Nonlinear Physics Center and ³Laser Physics Center, Research School of Physics and Engineering, The Australian National University, Canberra ACT 0200, Australia

⁴Centre de Physique Moléculaire Optique et Hertzienne, Université Bordeaux I, CNRS, 351 Cours de la Libération, 33405 Talence Cedex, France

[*volyar@crimea.edu](mailto:volyar@crimea.edu)

Abstract: We describe how the propagation of light through uniaxial crystals can be used as a versatile tool towards the spatial engineering of polarization and phase, thereby providing an all-optical technique for vectorial and scalar singular beam shaping in optics. Besides the prominent role played by the linear birefringence, the influence of circular birefringence (the optical activity) is discussed as well and both the monochromatic and polychromatic singular beam shaping strategies are addressed. Under cylindrically symmetric light-matter interaction, the radially, azimuthally, and spirally polarized eigen-modes for the light field are revealed to be of a fundamental interest to describe the physical mechanisms at work when dealing with scalar and vectorial optical singularities. In addition, we also report on nontrivial effects arising from cylindrical symmetry breaking, e.g. tilting the incident beam with respect to the crystal optical axis.

© 2010 Optical Society of America

OCIS codes: (260.1180) Crystal optics; (260.1440) Birefringence; (260.6042) Singular optics.

References and links

1. Q. Zhan, "Cylindrical vector beams: from mathematical concepts to applications," *Adv. Opt. Photon.* **1**, 1–57 (2009).
2. M. Stalder and M. Schadt, "Linearly polarized light with axial symmetry generated by liquid-crystal polarization converters," *Opt. Lett.* **21**, 1948–1950 (1996).
3. K. S. Youngworth and T. G. Brown, "Focusing of high numerical aperture cylindrical vector beams," *Opt. Express* **7**, 77–87 (2000), <http://www.opticsinfobase.org/oe/abstract.cfm?URI=oe-7-2-77>.
4. S. Quabis, R. Dorn, M. Eberler, O. Glockl, and G. Leuchs, "The focus of light—theoretical calculation and experimental tomographic reconstruction," *Appl. Phys. B* **72**, 109–113 (2001).
5. Q. Zhan and J. R. Leger, "Focus shaping using cylindrical vector beams," *Opt. Express* **10**, 324–331 (2002), <http://www.opticsinfobase.org/oe/abstract.cfm?URI=oe-10-7-324>.
6. F. Treussart, R. Alleaume, V. Le Floch, L. T. Xiao, J. M. Courty, and J.-F. Roch, "Direct measurement of the photon statistics of a triggered single photon source," *Phys. Rev. Lett.* **89**, 093601 (2002).
7. C. Varin and M. Piche, "Acceleration of ultra-relativistic electrons using high-intensity TM01 laser beams," *Appl. Phys. B* **74**, S83–S88 (2002).
8. T. Kuga, Y. Torii, N. Shiokawa, T. Hirano, Y. Shimizu, and H. Sasada, "Novel optical trap of atoms with a doughnut beam," *Phys. Rev. Lett.* **78**, 4713–4716 (1997).
9. J. J. McClelland and M. R. Scheinfein, "Laser focusing of atoms: a particle-optics approach," *J. Opt. Soc. Am. B* **8**, 1974–1986 (1991).
10. F. Gori, "Polarization basis for vortex beams," *J. Opt. Soc. Am. A* **18**, 1612–1617 (2001).

11. R. Borghi, M. Santarsiero, and M. A. Alonso, "Highly focused spirally polarized beams," *J. Opt. Soc. Am. A* **22**, 1420–1431 (2005).
12. R. Borghi and M. Santarsiero, "Nonparaxial propagation of spirally polarized optical beams," *J. Opt. Soc. Am. A* **21**, 2029–2037 (2004).
13. N. Passilly, R. de Saint Denis, K. Ait-Ameur, F. Treussart, R. Hierle, and J.-F. Roch, "Simple interferometric technique for generation of a radially polarized light beam," *J. Opt. Soc. Am. A* **22**, 984–991 (2005).
14. Z. Bomzon, V. Kleiner, and E. Hasman, "Formation of radially and azimuthally polarized light using spacevariant subwavelength metal strip grating," *Appl. Phys. Lett.* **79**, 1587–1589 (2001).
15. Z. Bomzon, G. Biener, V. Kleiner, and E. Hasman, "Radially and azimuthally polarized beams generated by space-variant dielectric subwavelength gratings," *Opt. Lett.* **27**, 285–287 (2002).
16. R. Oron, S. Blit, N. Davidson, and A. A. Friesem, "The formation of laser beams with pure azimuthal or radial polarization," *Appl. Phys. Lett.* **77**, 3322–3324 (2000).
17. D. J. Armstrong, M. C. Philips, and A. V. Smith, "Generation of radially polarized beams with an imagerotating resonator," *Appl. Opt.* **42**, 3550–3554 (2003).
18. H. Kawachi, Yu. Kozawa, and Sh. Sato, "Generation of radially polarized Ti:sapphire laser beam using a c-cut crystal," *Opt. Lett.* **33**, 1984–1986 (2008).
19. T. Fadeyeva, K. Kotlyarov, and A. Volyar, "Extreme spin-orbit coupling in Hermite-Gaussian beams in a uniaxial crystal," arXiv:0902.3716 (2009).
20. T. Fadeyeva and A. Volyar, "Extreme spin-orbit coupling in crystal-travelling paraxial beams," *J. Opt. Soc. Am. A* **27**, 381–389 (2010).
21. C. Loussert and E. Brasselet, "Efficient scalar and vectorial singular beam shaping using homogeneous anisotropic media," *Opt. Lett.* **35**, 7–9 (2010).
22. A. Shoham, R. Vander, and S. G. Lipson, "Production of radially and azimuthally polarized polychromatic beams," *Opt. Lett.* **31**, 3405–3407 (2006).
23. A. Niv, G. Biener, V. Kleiner, and E. Hasman, "Propagation-invariant vectorial Bessel beams obtained by use of quantized Pancharatnam-Berry phase optical elements," *Opt. Lett.* **29**, 238–240 (2004).
24. J. F. Nye, *Natural focusing and fine structure of light* (Inst. of Phys. Pub., Bristol, 1999).
25. D. W. Diehl, R. W. Schoonover, and T. D. Visser, "The structure of focused, radially polarized fields," *Opt. Express* **14**, 3030–3038 (2006), <http://www.opticsinfobase.org/oe/abstract.cfm?URI=oe-14-7-3030>.
26. R. W. Schoonover and T. D. Visser, "Polarization singularities of focused, radially polarized fields," *Opt. Express* **14**, 5733–5745 (2006), <http://www.opticsinfobase.org/oe/abstract.cfm?URI=oe-14-12-5733>.
27. Y. Luo and B. Lü, "Phase singularities of high numerical aperture radially and azimuthally polarized beams in the focal region," *J. Opt. A* **11**, 015707 (2009).
28. M. R. Dennis, K. O'Holleran, and M. J. Padgett, "Singular optics: Optical vortices and polarization singularities," *Prog. Opt.* **53**, 293–363 (2009).
29. J. Nye and M. Berry, "Dislocations in wave trains," *Proc. R. Soc. A* **336**, 165–190 (1974).
30. M. Soskin and M. Vasnetsov, "Singular optics," *Prog. Opt.* **42**, 219 (2001).
31. M. Vasnetsov and K. Staliunas, *Optical Vortices*, in *Horizons of World Physics* **228** (Nova Science, 1999).
32. Y. Izdebskaya, V. Shvedov, and A. Volyar, "Generation of higher-order optical vortices by a dielectric wedge," *Opt. Lett.* **30**, 2472–2474 (2005).
33. L. Allen, S. M. Barnett, and M. J. Padgett, "Optical Angular Momentum" (IOP Publishing, Bristol, 2003).
34. C. Alexeyev, A. Volyar, and M. Yavorsky, "Fiber optical vortices," in *Lasers, Optics and Electro-Optics Research Trends*, ed. L. I. Chen (Nova Science Pub., 2007) pp. 131–223.
35. T. Fadeyeva and A. Volyar, "Nondiffracting vortex-beams in a birefringent chiral crystal," *J. Opt. Soc. Am. A* **27**, 13–20 (2010).
36. A. Volyar and T. Fadeyeva, "Generation of singular beams in uniaxial crystals," *Opt. Spectrosc.* **94**, 264–274 (2003).
37. A. Volyar and T. Fadeyeva, "Decay and fusion of polarization umbilics of singular beam in crystal," *Opt. Spectrosc.* **95**, 285–29 (2003).
38. E. Brasselet, N. Murazawa, H. Misawa, and S. Juodkazis, "Optical vortices from liquid crystal droplets," *Phys. Rev. Lett.* **103**, 103903 (2009).
39. M. Born and E. Wolf, *Principles of Optics* (Pergamon, Oxford, 1975).
40. A. Ciattoni, G. Cincotti, and C. Palma, "Circular polarized beams and vortex generation in uniaxial media," *J. Opt. Soc. Am. A* **20**, 163–171 (2003).
41. A. Volyar and T. Fadeyeva, "Laguerre-Gaussian beams with complex and real arguments in uniaxial crystals," *Opt. Spectrosc.* **101**, 297–304 (2006).
42. I. Buinyi, V. Denisenko, and M. Soskin, "Topological structure in polarization resolved conoscopic patterns for nematic liquid crystal cells," *Opt. Commun.* **282**, 143–155 (2009).
43. Yu. Egorov, T. Fadeyeva, and A. Volyar, "The fine structure of singular beams in crystals: colours and polarization," *J. Opt. A* **6**, S217–S228 (2004).

44. A. Volyar, Yu. Egorov, A. Rybas, and T. Fadeyeva, "The fine structure of "white" optical vortices in crystals," *Tech. Phys. Lett.* **30**, 82–89 (2004).
45. V. Shvedov, W. Krolikowski, A. Volyar, D. N. Neshev, A. S. Desyatnikov, and Yu. S. Kivshar, "Focusing and correlation properties of white-light optical vortices," *Opt. Express* **13**, 7393–7398 (2005), <http://www.opticsinfobase.org/oe/abstract.cfm?URI=oe-13-19-7393>.
46. A. Volyar, V. Shvedov, T. Fadeyeva, A. S. Desyatnikov, D. N. Neshev, W. Krolikowski, and Yu. S. Kivshar, "Generation of single-charge optical vortices with an uniaxial crystal," *Opt. Express* **14**, 3724–3729 (2006), <http://www.opticsinfobase.org/oe/abstract.cfm?URI=oe-14-9-3724>.
47. V. Denisenko, V. Shvedov, A. S. Desyatnikov, D. N. Neshev, W. Krolikowski, A. Volyar, M. Soskin, and Yu. S. Kivshar, "Determination of topological charges of polychromatic optical vortices," *Opt. Express* **17**, 23374–23379 (2009), <http://www.opticsinfobase.org/oe/abstract.cfm?URI=oe-17-26-23374>.
48. V. Shvedov, Ya. Izdebskaya, A. Rode, A. S. Desyatnikov, W. Krolikowski, and Yu. S. Kivshar, "Generation of optical bottle beams by incoherent white-light vortices," *Opt. Express* **16**, 20902–20907 (2008), <http://www.opticsinfobase.org/oe/abstract.cfm?URI=oe-16-25-20902>.
49. D. Neshev, A. Dreischuh, V. Shvedov, A. S. Desyatnikov, W. Krolikowski, and Yu. S. Kivshar, "Observation of polychromatic vortex solitons," *Opt. Lett.* **33**, 1851–1853 (2008).
50. R. Beth, "Mechanical detection and measurement of the angular momentum of light," *Phys. Rev.* **50**, 115–125 (1936).
51. A. Ciattoni and C. Palma, "Anisotropic beam spreading in uniaxial crystals," *Opt. Commun.* **231**, 79–92 (2004).
52. T. A. Fadeyeva, A. F. Rubass, B. V. Sokolenko, and A. V. Volyar, "The vortex-beam 'precession' in a rotating uniaxial crystal," *J. Opt. A* **11**, 094008 (2009).
53. A. Ciattoni, G. Cincotti, and C. Palma, "Angular momentum dynamics of a paraxial beam in a uniaxial crystal," *Phys. Rev. E* **67**, 036618 (2003).
54. E. Brasselet, Ya. Izdebskaya, V. Shvedov, A. S. Desyatnikov, W. Krolikowski, and Yu. S. Kivshar, "Dynamics of optical spin-orbit coupling in uniaxial crystals," *Opt. Lett.* **34**, 1021–1023 (2009).
55. Ya. Izdebskaya, E. Brasselet, V. Shvedov, A. S. Desyatnikov, W. Krolikowski, and Yu. S. Kivshar, "Dynamics of linear polarization conversion in uniaxial crystals," *Opt. Express* **20**, 18196–18208 (2009), <http://www.opticsinfobase.org/oe/abstract.cfm?URI=oe-17-20-18196>.
56. A. Rubass, T. Fadeyeva, Yu. Egorov, V. Shvedov, A. Volyar, A. S. Desyatnikov, and Yu. S. Kivshar, "Spiral-like singular beams in gyrotropic crystals," *Proc. SPIE* **624**, 62540H-1-8 (2006).
57. G. N. Ramachandran and S. Ramaseshan, "Crystal optics" in *Handbuch der Physik* (Springer, Berlin, 1961).
58. T. Fadeyeva, A. Rubass, Yu. Egorov, A. Volyar, and G. Shvartzlander, "Quadrefringence of optical vortices in a uniaxial crystal," *J. Opt. Soc. Am. A* **25**, 1634–1641 (2008).
59. T. Fadeyeva, A. Rubass, and A. Volyar, "Transverse shift of high-order paraxial vortex-beam induced by a homogeneous anisotropic medium," *Phys. Rev. A* **79**, 053815 (2009).
60. F. Flossman, U. T. Schwarz, M. Maier, and M. R. Dennis, "Polarization singularities from unfolding an optical vortex through a birefringent crystal," *Phys. Rev. Lett.* **95**, 253901 (2005).
61. Ya. Izdebskaya, V. Shvedov, and A. Volyar, "Symmetric array of off-axis singular beams: spiral beams and their critical points," *J. Opt. Soc. Am. A* **25**, 171–181 (2008).

1. Introduction

One of the well studied phenomena in optics is the appearance of regular or irregular patterns in the distribution of polarization states of laser beams after passing through inhomogeneous or anisotropic media, e.g., optical fibers or birefringent crystals. In general, such a reshaping of the laser light impeded the practical applications of different optical devices and was considered undesirable, with much effort directed to weaken or to suppress at all the beam transformations, a representative example being the development of polarization maintaining optical fibers. This is however not always the case since light beams having space-variant polarization state can indeed exhibit fascinating properties that find important applications in various fields, see Ref. [1] for a review. Recently, with the progress in generation and control of radially and azimuthally polarized beams [2], the approach to the problem experienced a radical transformation. The laser beams carrying complex polarization states became a subject of active research because of their unusual focusing and propagation characteristics opening novel potential applications.

The *radially polarized* beams have axial symmetry in the sense that the electric vector points radially toward the optical axis at each point of the beam cross-section. The longitudinal component of the magnetic field vanishes in this case and the beam is of the transverse magnetic

field (TM-beam). As a result, the TM beam focused by a high numerical aperture lens forms a strong longitudinal component of the electric field [3]. The important fact is that the spot size near the focal plane of the TM beam associated with the longitudinal component is much smaller than that of the linearly polarized light [4] and the shape of the focal spot can be strongly tailored [5]. The unique properties of the radially polarized beams make them indispensable in different fields of modern physics, such as in optimization of photon collection efficiency of molecular-based single photon sources [6], in charged-particle acceleration [7], in guiding and trapping of particles [8], etc. The second type of the beams with unique properties is the *azimuthally polarized* beams [3]. The electric vector in such beams is perpendicular to the radial direction at each point of the cross-section and, consequently, the longitudinal component of the electric field vanishes (TE - beams). As a result, the azimuthally polarized beams can maintain the intensity zero at the beam axis and a complete cylindrical symmetry of the intensity distribution in the vicinity of the focal plane, even under the tight focusing, thus promising many useful wave structures for the atom lenses [9]. A new type of beams - the so-called *spirally polarized* beams that generalize the radially and azimuthally polarized beams, were introduced by Gori [10], and their focusing and propagation properties were studied in Refs. [11, 12].

Radially and azimuthally polarized beams are generally obtained from light fields having initially a uniform polarization state. One can mention the interferometric combination of orthogonally polarized beams (see, e.g., Ref. [13] and references therein), the propagation of the linearly polarized Gaussian beam through a twisted nematic liquid crystal [2] or subwavelength grating [14, 15], the intra-cavity mode generation with polarization-sensitive elements introduced into the laser cavity [16, 17], with the help of the specially fabricated optical fiber adjusted with the laser diode and phase plate [18], and recently introduced techniques using homogeneous uniaxial crystals illuminated by a circularly polarized higher-order Gaussian beams [19, 20] or a Gaussian beam shaped by axicons [21], achieving its total conversion into radially or azimuthally polarized beams. It is important to note that the radially and azimuthally polarized beams can be generated in polychromatic light [22] with the help of two conical reflectors and polarizing film. The beams with practically arbitrary distribution of polarization states can be shaped by means of quantized Pancharatnam-Berry phase optical elements produced by discrete computer-generated space-variant subwavelength dielectric gratings [23].

By definition, the polarization direction is undetermined, or singular, on the optical axis of a beam with radial or azimuthal polarization. The so-called *polarization dislocations* [24] appear in radially polarized and strongly focused beams [25–27] and they are linked to *phase dislocations* in the scalar fields, i.e. linear or circular polarization components of the vector beam [28]. Phase singularities were introduced more than three decades ago by Nye and Berry [29] and opened a new page of modern optics that came to be called singular optics [30]. The key object of singular optic is an *optical vortex*, which appears as an isolated point of total destructive interference, where the field amplitude vanishes while phase becomes uncertain. The wavefront in the vicinity of an optical vortex represents a helical surface with an integer number of the helix branches called topological charge l . The paraxial light beam bearing single ($l = \pm 1$) or multiple charge ($|l| > 1$) optical vortex is usually produced using computer-generated hologram technique [31]. Other relatively simple ways to produce vortex beams employ spiral phase plates in the form of a helix surface engraved on the transparent plate [31] or the diffraction on a dielectric wedge [32]. One of the most intriguing properties of twisted wavefront is the appearance of the optical orbital angular momentum (OAM) of the beam L_z [33].

The total angular momentum (TAM) of a light field M_z , however, has also an independent contribution arising from its polarization state, namely the circular polarization is associated with the spin angular momentum S_z (SAM) [33] directed along the optical z -axis. Therefore the TAM of a paraxial optical vortex that propagates along the z axis in free space or isotropic

homogeneous medium can be written as $M_z = L_z + S_z$, which is conserved in the absence of absorption.

A drastically different situation occurs when the beam propagates in birefringent medium. The OAM and SAM are strongly coupled with each other forming modal states. It is worth noting that a superposition of the *radially* and *azimuthally* polarized beams (TE and TM modes) forms a vortex beam with a uniformly distributed circular polarization. However, such a combined vortex-beam has a zero angular momentum because the SAM and OAM have the same amplitudes and opposite signs. As a rule, these mode combinations cannot independently exist in an anisotropic medium because they decay into simple wave states in the form of pure TE and TM modes [34]. The exception is birefringent chiral crystals where the eigen-modes are *spirally* polarized beams built as specific combination of TE and TM modal beams [35]. In contrast, a vortex beam with the same signs of the OAM and SAM cannot be described in terms of the radially and azimuthally polarized beams and is stable in different types of anisotropic media [34].

Contrary to the most common techniques to create vortex beams, such as computer generated holograms or spiral phase plates, the use of a birefringent anisotropic medium can naturally engineer a complex polarization distributions with inclusions of polarization singularities [24] that can carry an array of optical vortices in one of the polarization components [36, 37]. Such a concept of natural engineering has been recently shown to enable drastic downsizing of singular optical devices when using self-organized anisotropic materials such as liquid crystals, as demonstrated by the realization of micron-scale liquid crystal droplets optical vortex generator [38]. Although the propagation of plane waves in a birefringent uniaxial media was considered in details in the beginning of the last century in the framework of the Fresnel formulas [39], the beam propagation as a superposition of plane waves has been only recently analyzed on the basis of paraxial wave equation [40–42]. It is noteworthy that even in a general case of a light field passing through a homogeneous birefringent crystal the polarization distribution develops distinct singularities. There are three major types of the polarization singularities [24] in a complex vector field: the *star*, the *lemon* and the *monstar*. The points in space that correspond to polarization singularities (the so-called C-points) have either the right-hand circular polarization (RCP) or the left hand circular polarizations (LCP) so that one of the circularly polarized field components vanishes. They are described by the topological index s that characterizes the number of the revolutions of the polarization ellipse major axis when circling around the polarization singularity: the star has the index equal $s = -1/2$, while for lemon and monstar $s = 1/2$. When the vector field is subjected to some perturbations, the lemon can be transformed into the monstar and vice versa [37, 42]. The C-points are divided between each other by the line of linear polarizations, the so-called L-lines [28].

In this paper, we describe physical mechanisms of shaping the spatial distribution of polarization states of laser beams passing through birefringent media. We distinguish two main approaches, described in Sections 2 and 3, respectively. The first one relates to the on-axis propagation of the beams, which can be described by superposition of modal TE and TM beams. We discuss generation of white-light (broadband or supercontinuum) optical vortex beams, spin-orbit coupling, and the effect of chirality of crystal's dielectric permeability. In contrast, the consequences of breaking the cylindrical symmetry of the light-matter interaction by the oblique illumination are discussed in Sec. 3, including single charge optical vortex generation and beam quadrefringence. Section 4 concludes the paper.

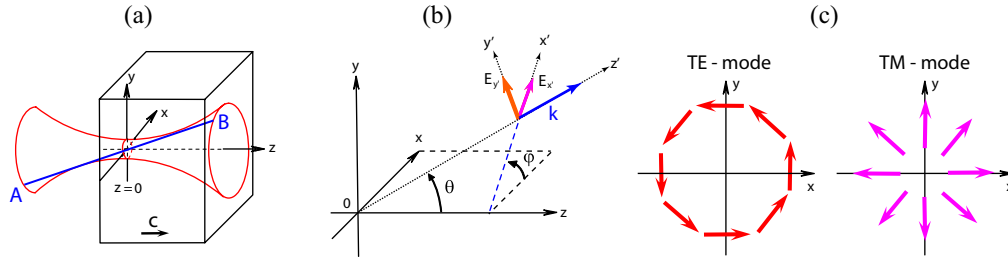


Fig. 1. (a) On-axis propagation of a Gaussian beam; \mathbf{c} is a unit vector that defines optical axis z . (b) Shaping of the TE and TM eigen-modes; corresponding directions of the electric field are indicated in (c) with arrows.

2. On-axis propagation

2.1. Radially and azimuthally polarized eigen-mode beams

Here we discuss the main processes at work when a uniformly polarized incident light beam propagates along the optical axis of a uniaxial crystal [36,37,41]. Figure 1 illustrates the on-axis beam propagation with Gaussian envelope through the crystal. We assume that the refractive indices along the major crystallographic axes x, y, z are n_o, n_o, n_e , respectively. Let us consider the ray AB that intersects the origin of the reference frame $\{x, y, z\}$ so that the plane zOz' involving the ray and the crystal optical axis \mathbf{c} is tilted at the angle φ to the xOz plane, see Fig. 1(a). The linear polarization component with the envelope $E_{x'}$ lies in the plane zOz' while $E_{y'}$ component is perpendicular to this plane [39], see Fig. 1(b). In the paraxial approximation, we can assume that the projections of the $E_{x'}$ and $E_{y'}$ components onto the xOy plane are equal to each other: $E_{x'} \approx E_x$, $E_{y'} \approx E_y$. Because of the cylindrical symmetry the $E_{x'}$ components of all rays form the field of the azimuthally polarized TE mode beam or the *ordinary beam*, while the $E_{y'}$ components form the radially polarized TM mode beam or the *extraordinary beam*, see Fig. 1(c). Both beams propagate along the crystal optical axis having the same phase velocities characterized by the wave number $k_o = k_0 n_o$, where k_0 stands for the wavenumber in free space. However, the Gaussian envelopes have different wavenumbers k_o and k_e . The exact value of the k_e wavenumber in the beam envelope derived from the solution to the paraxial wave equation [40,41] is $k_e = (n_e^2/n_o)k_0$. Thus, the beam with the uniform polarization distribution at the input plane $z = 0$ of the crystal can be decomposed as a superposition of the azimuthally (TE) and the radially (TM) polarized beams. As they propagate through the crystal, the complex amplitudes of the TE and TM beam are transformed by different ways shaping a regular pattern of the polarization distributions at the crystal output. Nevertheless, we can regard the TE and TM beams as the modal beams with eigen-polarization since they do not change their structure up to the scale transformation due to diffraction. It is important to note that the description of the beam behavior depends on the polarization basis of the beam representation. If the linearly polarized components are detected after the crystal, it makes sense to present the eigen-mode beams in the linearly polarized basis $\{\mathbf{e}_x, \mathbf{e}_y\}$: $|TE\rangle \sim \mathbf{e}_x y - \mathbf{e}_y x$ and $|TM\rangle \sim \mathbf{e}_x x + \mathbf{e}_y y$. From whence we find that the polarization components have the edge dislocations [29] along the x - or y -axes. If the circularly polarized components are detected after the crystal, the field can be conveniently rewritten in the circularly polarized basis $\{\mathbf{e}_+, \mathbf{e}_-\}$: $|TE\rangle \sim r(\mathbf{e}_+ e^{-i\varphi} - \mathbf{e}_- e^{i\varphi})$ and $|TM\rangle \sim r(\mathbf{e}_+ e^{-i\varphi} + \mathbf{e}_- e^{i\varphi})$. The last expression means that the circularly polarized components of the TE and TM modes carry the single-charge optical vortices with opposite signs of the topological charges.

Let us consider the propagation of a circularly polarized beam through the crystal [37] de-

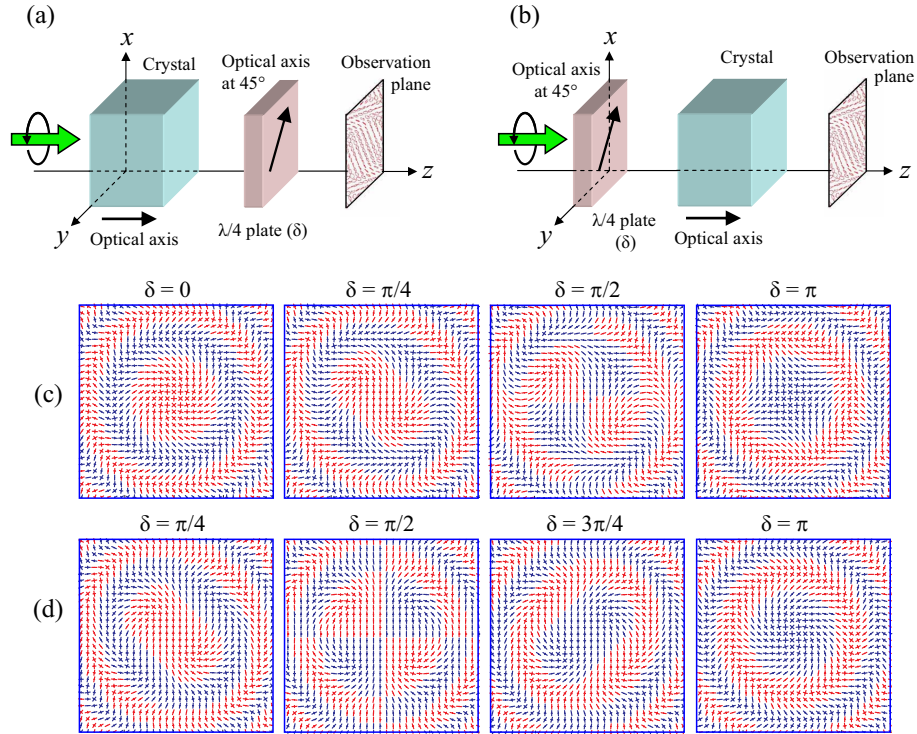


Fig. 2. Optical arrangement used for polarization shaping of an incident beam with uniform circular polarization and two kinds of combination for a c-cut crystal and a phase plate, which introduce a phase delay δ between direction at $\pm 45^\circ$ from the x and y axis. The spatial distribution of the polarization state is made in the observation plane after the two anisotropic optical elements. The geometries shown in (a) and (b) correspond to polarization distributions in (c) and (d), respectively, with the values of phase difference δ indicated. The ellipses of RCP (red) and LCP (blue) are shown by their main axes.

pictured in Fig. 2(a). The crystallographic axes \mathbf{o} and \mathbf{e} of the phase plate are tilted by the angle $\phi = \pi/4$ in the reference frame $\{x, y\}$. The phase plate is introduced to manipulate the polarization distribution produced by the crystal; the additional polarization filter (the quarter-wave plate and polarizer) is not shown because it does not take part in shaping the field and used only for measuring the polarization distributions. The phase plate introduces the phase shift δ between the electric vector components while the rotation angle ϕ provides the entanglement of the polarization components. The parameter δ is a phase retardation between the ordinary and extraordinary waves in the phase plate, for example $\delta = \pi/2$ for the quarter-wave plate. In general, this parameter can be varied using different means, e.g. the electro-optic effect.

The polarization distributions of the fields in the schemes in Figs. 2(a), 2(b) can be calculated using exact solutions to parabolic wave equation, yet the later have a rather cumbersome form and inconvenient to use. However, similar patterns can be also calculated with the approximate technique of the far field employed in Ref. [34] or transformation matrix in Ref. [54]. In this case we can use the Jones formalism and corresponding Jones matrix for the phase plate in the basis of circular polarizations:

$$\hat{\Phi} = \begin{pmatrix} \cos(\delta/2) & i \sin(\delta/2) \exp(-i2\phi) \\ i \sin(\delta/2) \exp(i2\phi) & \cos(\delta/2) \end{pmatrix}. \quad (1)$$

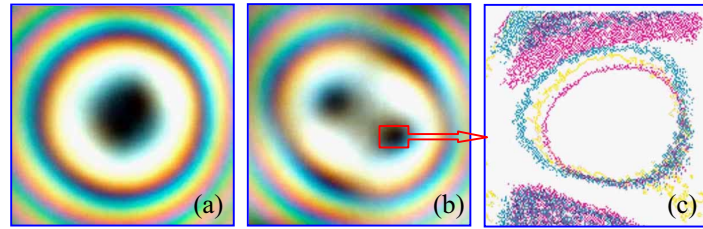


Fig. 3. (a) Degenerated white optical vortex; (b) splintered white optical vortices; (c) color distributions in the vicinity of the shifted vortex core [43].

The polarization distributions shown in Fig. 2(c) illustrate the field transformations when changing the phase shift δ produced by the phase plate. When the phase shift is zero, $\delta = 0$, the crystal forms the field with the degenerated C-point positioned at the beam axis, its topological index is one, $s = 1$. The centered singularity is encircled with numerous degenerated C-lines with the alternate right and left circular polarizations. The phase plate perturbs the field after the crystal and removes the degeneracy of the centered C-point so that it decays into two lemons. At the same time, each degenerated C-line decays into two stars and two monstars, the monstars being converted into lemons with increase of the phase shift up to $\delta = \pi/4$. At the phase shift $\delta = \pi/2$, two lemons originated from the centered C-point and two stars from the degenerated C-line form a sort of the symmetrical vector topological quadrupole near the beam axis. The numerous quadrupoles far from the beam axis are shaped in the same way. Then two lemons from the first quadrupole and two stars from the second quadrupole start to gather together uniting again into the degenerate C-line at the phase shift $\delta = \pi$. At the same time, two stars from the first quadrupole form the degenerated C-point at the beam axis. Noteworthy that centered C-point at $\delta = 0$ is associated with the double-charged optical vortex embedded in the LCP field component if the initial beam is right hand polarized. Moreover, the sign of the vortex charge, which is controlled by the handedness of the circularly polarized light beam entering into the crystal, does not change at the phase shift $\delta = \pi$.

The transposition of the crystal and the phase plate, when the crystal is positioned after the phase plate in Fig. 2(b), results in shaping new patterns of the polarization states shown in Fig. 2(d). The major distinctive feature of the field distributions in comparison with the previous case [Fig. 2(c)] is that the beam fields at the phase shift $\delta = 0$ and $\delta = \pi$ are associated with the double charge vortices in the orthogonally polarized components with opposite signs of the topological charges. It means that the sign of the vortex topological charge is converted into the opposite one when changing the handedness of the circular polarization in the initial light beam. Naturally, the polarization filter positioned after the crystal and the phase plate enables us to visualize the optical vortices hidden in the polarization singularities controlling their spatial positions. In the general case, the vortex topological charges in the circularly polarized components differ by two units [40, 41]. The detailed experimental results presented in the papers [36, 43, 44] are in a good agreement with the above theoretical representations.

2.2. White optical vortices

The unique property of the crystal to shape the symmetrical distributions of the polarization states with the degenerated C-point at the beam axis with the topological index $s = 1$ do not depends on the wavelength of the beam. It means that the positions of the optical vortices in the LCP component coincide independently of the wavelength. Such a beam quality was employed by us to generate experimentally the polychromatic or *white optical vortices*, see Refs. [36, 43–49] and references therein. The white optical vortices can be generated with the

help of the experimental set-ups shown in Figs. 2(a), 2(b), but with an additional polarization filter consisting of a quarter-wave plate and a linear polarizer and able to filter out the circular polarized components or their composition [54, 55]. The light source was a halogen lamp whose radiation is launched into the optical fiber and then collimated by the lens system. The major difficulty was in the separation of the white optical vortex from the total light flux. To this end, we have employed the Fresnel's rhomb in the first experiments [36, 43–46] to create a circularly polarized light and to separate the orthogonally polarized components but later it was substituted by the achromatic quarter-wave plate [47, 48]. Figures 3(a), 3(b) illustrate intensity distributions of the experimentally created [36, 43–45] polychromatic beams bearing the white optical vortices. The core of the centered optical vortex in Fig. 3(a) is slightly deformed. The vortex deformation is caused by a not-total compensation of the phase difference for different wavelengths in the Fresnel's rhomb. The deformation increases when splitting the degenerated vortex into two single charge vortices, see Fig. 3(b). The corresponding level-lines for different colors in vicinity of the shifted vortex core in Fig. 3(c) show that a displacement of the white vortex from the center entails blurring the field zero at the vortex center for account of different positions of the monochromatic vortices. This robust technique was used for experimental generation of polychromatic single- and double-charge optical dark vortex solitons in a lithium niobate crystal, the latter employed as a nonlinear medium with defocusing nonlinearity [49].

2.3. The spin-orbit coupling

The generation of a double charge on-axis optical vortex when circularly polarized beam propagates along the optical axis of a (transparent) uniaxial crystal embraces a fundamental phenomenon that involves the conservation of the light angular momentum flux. As a matter of fact, the total angular momentum of the paraxial beam is conserved for any direction of the beam propagation in free space or optical transparent homogeneous and isotropic medium [33]. However, a birefringent medium transforms both the beam polarization and its shape and, consequently, changes the OAM and SAM of the beam (see, e.g. Refs. [50–52]). However, Ciattoni et al. have showed that the projection of the angular momentum flux onto the beam axis is conserved [53]. Thus, when propagating the beam, the OAM and SAM are transformed but the regulatory mechanism is accomplished by the *spin-orbit coupling*. We have experimentally and theoretically studied this effect [54, 55] in the uniaxial calcite crystal samples that are cut perpendicularly to the optical axis into thin slabs both for the monochromatic and polychromatic vortex-free Gaussian beams at the crystal input. The curves in Fig. 4(a) trace the behavior of the SAM and OAM in the circularly polarized components of the beam (with the right hand circular polarization at the crystal input) along the crystal length. The vortex-free beam at the crystal input has the unit spin angular momentum flux [solid and dashed red curves in Fig. 4(a)] $S_z = 1$ and the zero orbital angular momentum [green curve in Fig. 4(a)]. As the beam propagates through the crystal, the depolarization process decreases the spin angular momentum flux as a whole, i.e., $S_z(z \rightarrow \infty) \rightarrow 0$. Since the total angular momentum (TAM) flux is conserved, the polarization changes are associated with the generation of a double charge optical vortex embedded in the circularly polarized component of the field with opposite handedness with respect to the incident circular polarization state. Consequently, the contribution of the OAM to the TAM increases along the propagation, as shown in Fig. 4. At the relatively large crystal length, it tends to unity, $L_z(z \rightarrow \infty) \rightarrow 1$, and the balance of the total angular momentum flux along the z -axis is recovered, $S_z(z) + L_z(z) = 1$, for any crystal cross-section.

The efficiency of the spin-orbit coupling can be described by the ratio $\eta = (1 \mp S_z)/2$, where the minus sign is associated with the RCP at the crystal input, while the plus sign corresponds to the left-handed initial polarization. Thus, the asymptotic value is equal to $\eta(z \rightarrow \infty) = 1/2$ for the case of the considered above Gaussian beam. But can the *spin-orbit efficiency* η exceed

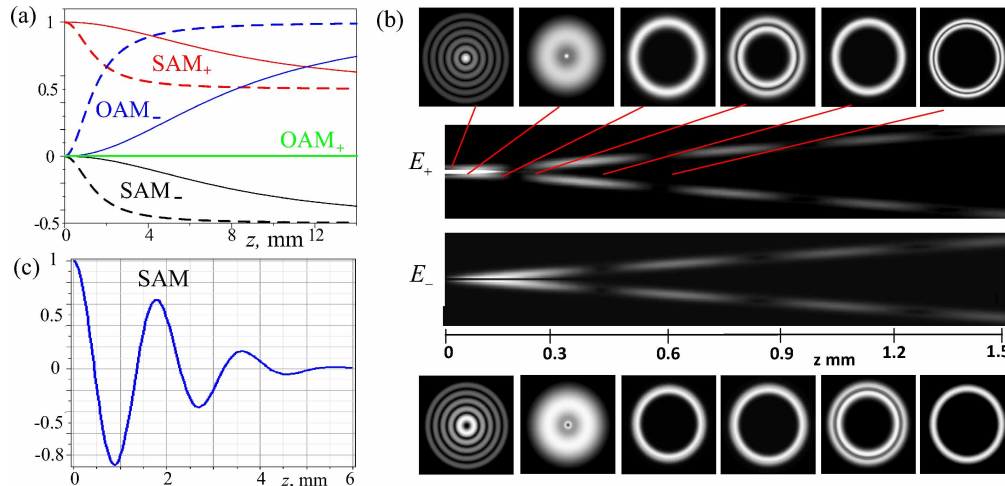


Fig. 4. (a) The spin (SAM) and orbital (OAM) angular momenta for the circularly polarized components of the Gaussian beam with waist $4.6\ \mu\text{m}$ (dashed lines) and $11\ \mu\text{m}$ (solid lines) [54]. (b) Intensity distributions of the circularly polarized field components and (c) spin momentum of the Bessel-Gaussian beam of the lowest order $l = 0$ in LiNbO_3 crystal [20].

the value $\eta = 0.5$ and reach hundred percent $\eta = 1$ at the finite crystal length? We have shown that such a situation can be practically realized by using higher-order Gaussian beams [20] as well as an incident fundamental Gaussian beam that has been shaped by axicons [21], with almost 100% efficiency reached when the half-wave plate condition is satisfied.

Indeed, there is a number of paraxial beams whose field structure is transformed when propagating, e.g. the Hermite- and Laguerre-Gaussian beams with the complex argument (see, e.g., Ref. [41] and references therein). Such a property is also inherent to the Bessel-Gaussian beams. Figure 4(b) shows the transformations of the intensity profile of the Bessel-Gaussian beam of the lowest order $l = 0$. At the initial part of the beam length, the annular structure in both, the RCP and LCP components, is quickly transformed into one ring. The phase difference between the ordinary and extraordinary beams is insufficient to change globally the intensity distribution. At some crystal length, typical conoscopic pattern starts to take shape. For the beam with a smooth axially symmetric field distribution, as in classical experiments [39], the conoscopic pattern has the form of concentric rings. However, the field with the only narrow circular intensity peak in Fig. 4(b) acquires only one dark ring. At the same time, a total intensity of the RCP component is sharply reduced while the total intensity of the LCP component grows. Further, the former ring structure is recovered in the RCP component whereas the LCP component gets a dip in the intensity distribution and a sharp decreasing of the total intensity. Then the process is resumed along the crystal length. A maximum energy transport [and, consequently, the peak of the SAM shown in Fig. 4(c)] takes place when the condition of the phase matching is fulfilled, i.e. the phase difference is equal to π between the ordinary and extraordinary beams at a small area corresponding to the intensity ring and their curvature radii of the wavefronts are equalized. It is important to note that the extreme spin-orbit coupling is not inherent in the standard Hermite- and Laguerre-Gaussian beams with a real argument.

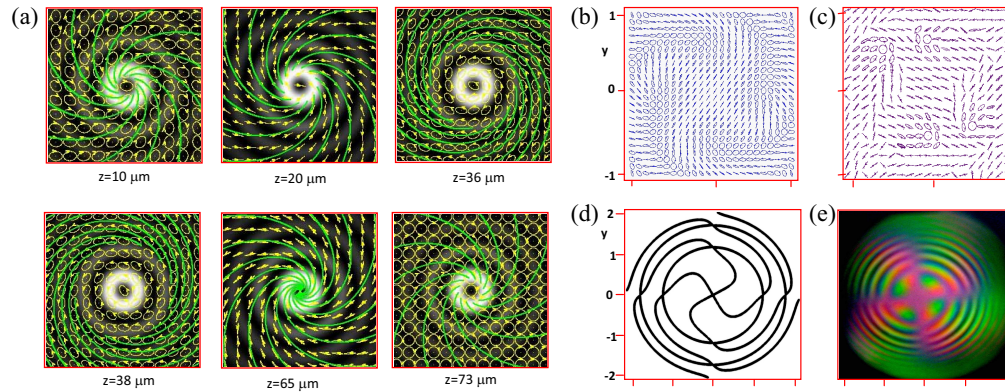


Fig. 5. (a) Maps of the polarization states on the background of the intensity distribution of a Bessel beam; the curves show the directions of the major axes of polarization ellipses [35]. (b) Theoretical and (c) experimental maps of the polarization states, and (d) the theoretical edge dislocation lines for the monochromatic light. (e) Experimental intensity distribution of the polychromatic light from a halogen lamp for the Gaussian beam after the system of two SiO₂ birefringent chiral crystals with opposite signs of chirality [56].

2.4. Spirally polarized beams in birefringent chiral crystals

Birefringent chiral crystals are especially suitable media for the generation spirally polarized beams [35, 56] benefiting from the combined affects associated to linear and circular birefringence (the latter refer to optical activity). Indeed, the optical activity of a chiral crystal makes the major axis of the polarization ellipse of each of the plane waves that participate to the coherent superposition in the frame work of an integral representation of the optical field. In practice, Bessel light beams, which can be described as conical bundle of plane waves, are well-suited to illustrate the influence of birefringent chiral crystals on light. This has been done in the paper [35], where the behavior of non-paraxial Bessel beams have been considered. Without going into calculation details, we note that a single birefringent chiral uniaxial crystal can display a number of unexpected properties relative to the nonparaxial beam, for example the transformation of a uniformly polarized beam into a spirally polarized one. The fields of the eigen-modes are of the superposition of the azimuthally and radially polarized beams propagating with different propagation constants β_+ and β_- : $\mathbf{E}^\pm = (\mathbf{E}_{TE} + B_\pm \mathbf{E}_{TM}) \exp(i\beta_\pm z)$, where B_\pm are the ratios between the amplitudes of the two eigen-fields. Figure 5(a) shows the maps of the polarization states at the output of a purely chiral crystal (i.e., without linear birefringence) for an incident circularly polarized non-paraxial Bessel beam, which is superimposed on the intensity distribution profile. In this figure, the solid lines are tangential to the major axis of the polarization ellipse at each point of the electric field. As a matter of fact, the incident beam undergoes significant non-uniform polarization changes even for short propagation distance inside the crystal. Gradually the polarization ellipses at each point of the beam cross-section are pulled out, transforming into a spirally polarized field with the right handedness of the integral curves when transmitting the beam. Consequently, the beam gets uniformly polarized. The further beam propagation results in formation of the spirally polarized beam with the left handedness at the definite crystal length.

The most interesting beam transformations manifest themselves in the system of two birefringent chiral crystals having chirality of opposite signs. The property of such a combination of crystals to form a fyfot-like intensity distribution (the so-called *Airy spirals*) is well-known from the end of the nineteenth century [57]. However, the detailed analysis of the singular field

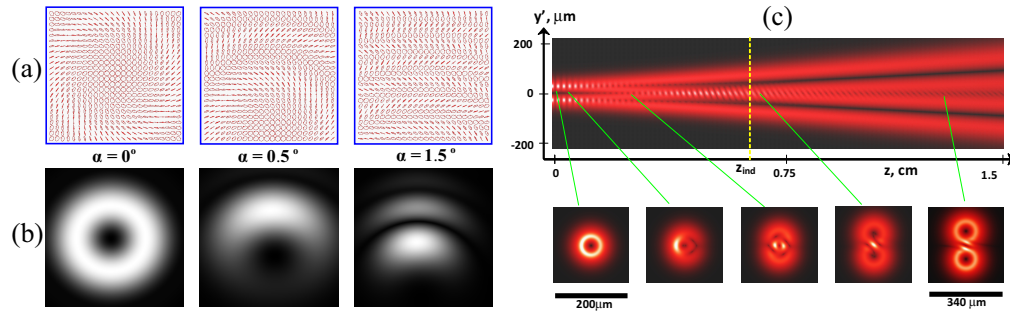


Fig. 6. Output polarization (a) and intensity (b) distributions of the circularly polarized field component orthogonal to the incident circularly polarized Gaussian beam impinging at oblique incidence onto a c-cut crystal. (c) Splitting of the left-handed beam component at the inclination angle $\alpha = 10^\circ$ [59].

structure for paraxial beams has not been performed. In the paper [56] we have analyzed the field transformations of the vortex-beams (including the vortex-free Gaussian beam) passing through two birefringent chiral crystals with opposite chirality both for the monochromatic and polychromatic light. The theoretical and experimental maps of the polarization states, shown in Fig. 5(b), 5(c), are of the field distributions obtained for the system of two SiO₂ crystals with the opposite signs of the chirality provided that the linearly polarized light with electric vector tilted at the 45° to the axes of the referent frame, is launched into the crystal system. The characteristic features of the maps are the vector topological quadrupole consisting of four polarization singularities (two stars and two lemons) positioned at the bends of the L-lines (the lines with a linear polarization). These lines form a system of the concentric rings and the double spiral. After passing through a linear polarizer the spiral-like pattern of the edge dislocations shown in Fig. 5(d) is shaped at the beam cross-section; the output intensity pattern, shown in Fig. 5(a), in the case of a polychromatic light exhibits a typical Airy spiral pattern, as shown in Fig. 5(e).

3. Oblique propagation

In previous Section, the singular beam shaping using uniaxial crystals has only been considered under light propagation along the optical axis of a c-cut crystal. Here, we will discuss the consequences of oblique propagation of light with respect to the optical axis of the crystal. For this purpose we further consider paraxial beams at small oblique incidence of the optical axis of a uniaxial crystal, which has been treated in the papers [50,56,59,60] both from a theoretical and experimental point of view. More specifically, the topological aspects of the problem were analyzed by Flossman et al. [60], employing a simple model of two linearly polarized beams.

Let us consider the field transformations in the Gaussian beam with the initial RCP whose axis is tilted at the angle α to the crystal optical axis [59]. The maps of the polarization states, intensity distributions in the LCP component, and corresponding interference patterns are shown in Fig. 6(a), 6(b). Even a slight inclination of the beam results in the displacement of the degenerated polarization singularity and its splitting into two lemons. It associated with sliding of the double charged optical vortex in the LCP component off the crystal axis and splitting it into two single charge ones that move down, see Fig. 6. The beam cross-section is strongly deformed with tilting. The details of the process are described in the papers [58, 59], but we focus our attention here on the major features that can be illustrated by Fig. 6(c) on the example of the RCP initial beam bearing the negatively charged optical vortex $l = -1$ (the beam incli-

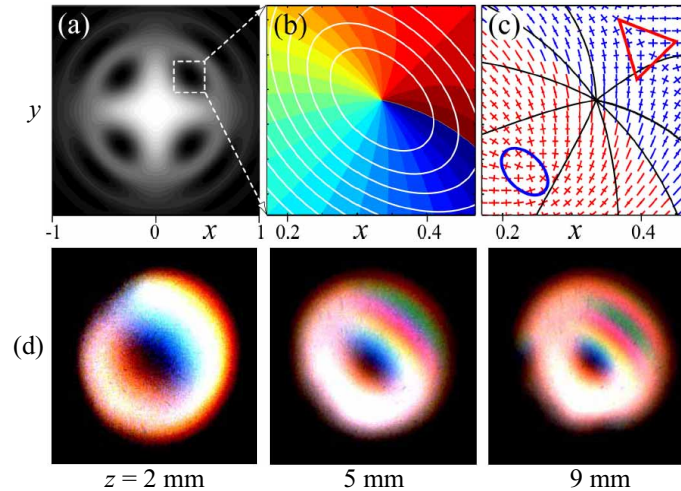


Fig. 7. Numerically calculated (a) intensity and (b) phase profiles of the on-axis x -polarized field component at 6 mm propagation length; white lines in (b) show intensity contours [46]. (c) The polarization map of the total transmitted field with ellipses of the left-hand (red) and right-hand (blue) polarizations indicated by their main axes. Blue ellipse and red triangle indicate the monstar and star polarization singularities and black lines show the phase contours in (b). (d) Experimentally measured output white-light intensity profiles with optimal input angle α for different propagation distances, as indicated [55].

nation is shown in the referent frame connected with the tilted axis of the initial beam). The beam inclination does not immediately lead to the splitting of the initial circularly polarized beam into two linearly polarized ones, as could be seen from the traditional representations for plane waves [39]. The ordinary and extraordinary polarized beam components propagate together along the optical axis of the initial tilted beam. Yet the intense dislocation reactions takes place in the composite beam - the birth and annihilation of the set of optical vortices. The optical vortices are jumbled up in the beam so that we cannot point out which optical vortex belongs to which component. However, starting at some distance z_{ind} (that came to be called the *indistinguishability limit* [58]) the vortices “choose” their own specific beam and the ordinary and extraordinary beams in both circularly polarized components split. The topological charges of the splintered off-axis beams in the LCP components differ from those in the on-axis beam. The partial beams acquire now the optical vortices with the same topological charges. The double charged vortex disappears in the combined beam taking away the orbital angular momentum. Besides, the beam becomes depolarized, i.e. it loses also the spin angular momentum. However, the tilted beam acquires new properties and we will focus below on two of them: the generation of single charged vortices and the beam quadrefringence.

3.1. Generation of single charge vortex beams

Let us consider the propagation of a linearly polarized Gaussian beam tilted at the angle α to the crystal optical axis [46, 55, 59]. The initially linearly polarized beam can be described as a sum of two circularly polarized ones with opposite handedness. The RCP (LCP) component of the incident field is partly converted into a LCP (RCP) component in which is embedded a phase singularity with topological charge $l = -2$ ($l = +2$), as discussed in detail in Sec. 2. Therefore, inside (and also at the output) of the crystal, the beam contains a mixture of optical vortices with topological charges ± 2 in each of the linearly polarized components E_x and E_y . When $\alpha \neq 0$,

the double charge phase singularity leaves the beam, as illustrated in Fig. 6(b), and the beam acquires a non-uniform spatial polarization distribution, see Fig. 6(a). As a consequence of a conservation of the TAM for the light field, the ordinary and extraordinary components of the field have to be tilted and shifted apart from each other [59] (see next section), which leads to the formation of an array of single charge optical vortices [61]. This process results in the typical intensity and phase distributions of the electric field replicating the local distribution around one of the singularities in topological quadrupole for the on-axis beam, shown in Figs. 7(a) and 7(b), respectively. The polarization pattern contains two kinds of polarization singularities: the monstar and the star, positioned at the maximum values of the field component polarized at the 45° , see Fig. 7(c). The singularities are divided between each other by the L-line and the direction of the linear polarization rotates very quickly along this line. For $\alpha \neq 0$, the zero of linear polarization directed at the angle 135° is positioned at the center of the tilted beam. When we go around this point on the clockwise direction retracing the angle of rotation of the polarization ellipse, we find its rotation angle equal to -180° (taking into account the degeneracy of the 180° and 360° - directions). It means the topological index of the point to be $s = -1/2$. Besides, the field component with a linear polarization directed at the 45° vanishes at the beam center. Thus, this beam component carries a single charge optical vortex.

For a beam tilted at given angle α , a single charge optical vortex is nucleated on the edge of the $E(45^\circ)$ field component and at some propagation length its origin coincides with the beam center while with further propagation vortex moves away from the beam. Similar situation is observed when the crystal length is constant while the inclination angle changes. Therefore, for a given crystal length there is an optimal inclination angle when the output beam contains an isolated single charge vortex on its axis. It is noteworthy that the same method enables us to create the single charge vortices embedded in the polychromatic beams for different crystal lengths, the experimental results for polychromatic light [55] are shown in Fig. 7(d). In contrast to the centered double charge vortices in the polychromatic on-axis beams that have the axially symmetric rainbow colouring around the vortex core, the vortex core in the tilted polychromatic beams is blurred because the positions of the L-line are different for different wavelength. The vortex core gets the asymmetrical colouring.

3.2. The beam quadrefringence

Let us focus on the case when the tilted beam is split into two ordinary and extraordinary partial beams forming two doughnut beams as shown in Fig. 8(a). For convenience, we assume that the initial beam is right-handed circularly polarized and carries a triple-charged optical vortex with topological charge $l = -3$. If the beam propagates along the crystal optical axis it has the single charge vortex $l = -1$ embedded in the LCP component [36, 43]. When tilting the beam at the inclination plane $y0z$, the topological charges in the RCP and LCP components are equalized [59], i.e. the LCP component gets the additional optical vortex with the topological charge $l = -2$. Besides, the beam as a whole is depolarized. Thus, the initial beam had the OAM flux $L_z = -3$ and the SAM flux $S_z = +1$ so that the total angular momentum flux at the input crystal face is $L_z(z=0) + S_z(z=0) = -3 + 1 = -2$. In the asymptotic case $z \rightarrow \infty$, the beam OAM flux is $L_z(z \rightarrow \infty) = -3$, but the SAM flux vanishes $S_z(z \rightarrow \infty) = 0$ due to the depolarization so that the total angular momentum flux $L_z(z \rightarrow \infty) + S_z(z \rightarrow \infty) = -3 + 0 = -3$. The balance of the angular momentum flux is violated! To keep the balance [53], the beam must get the additional angular momentum flux $\Delta M = +1$ so that $L_z(z=0) + S_z(z=0) = L_z(z \rightarrow \infty) + S_z(z \rightarrow \infty) + \Delta M = -2$. Such an additional ΔM , the beam acquires from the transverse shift Δx of the center of gravity of the beam relative to the initial beam axis $\Delta M = k\alpha\Delta x = 1$ [59] (where k is the wavenumber) in the direction $0x$ perpendicular to the inclination plane $y0z$. But the vortex structure of the RCP component E_+ does not change. The transformation is

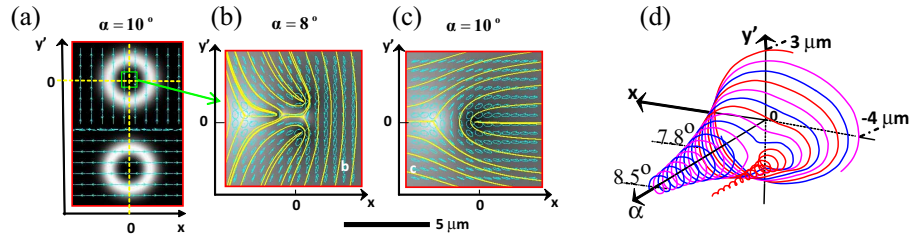


Fig. 8. (a) Intensity and (b, c) polarization distributions in the splintered partial beams in the LiNbO_3 crystal on the background of the distribution of the ellipticity (gray scale from -1 to 1) of the polarization states. The initial beam has the right-hand polarization and the centered optical vortex with the topological charge $l = -3$. (d) The key fragment of the vortex trajectories in the LCP component for the initial triple-charge vortex beam [59].

experienced only by the LCP component E_- . Consequently, the center of gravity of the LCP component is shifted relative to the RCP component by the distance $\Delta x = 2/(k\alpha)$. Noteworthy is that such a lateral shift does not depend on the vortex topological charge l of the initial beam (including the vortex-free Gaussian beam) and is defined exclusively by the incident circular polarization and tilt angle α .

Thus, the circularly polarized beam in the crystal experiences birefringence, being split into the ordinary and extraordinary polarized beams. Each component is split in turn into two beams at the expense of a transverse shift of the LCP component so that the input beam in the crystal experiences a *quadrefringence* [58, 59]. However, the value of the lateral displacement is very small (about the wavelength) and it can be neglected in practice.

Let us consider briefly the physical mechanism of the transverse shift [58, 59]. To this end we must peer into the darkness of the central region of the beam, as shown in Fig. 8(a). At the first glance, it seems that the splintered beams in Fig. 8(a) have a uniform linear polarization along the x - and y -axes. However, in the vortex core the beam is non-uniformly polarized. It has a complex structure consisting of a number of polarization singularities - the star and lemons [Fig. 8(b)]. With the increase of the inclination angle α [Fig. 8(c)], three lemons and two stars gather together forming the only lemon-like polarization singularity while one star is removed along the x -axis. The positions of these singularities do not coincide for any crystal length. The trajectories of corresponding scalar optical vortices in the LCP component are shown in Fig. 8(d), in coordinates $\{x, y', \alpha\}$. All vortex trajectories are very close at first, before one optical vortex splits off from the rest, tracing its own trajectory. The two remaining vortices approach each other gradually and ultimately form a smooth central vortex trajectory. The vortex splitting results in shifting of the center of gravity of the LCP component. The trajectory of the center of gravity has the simplest structure for the vortex-free Gaussian beam, its oscillation is caused by the dislocation reactions in the beam components. The oscillations are ceased after passing through the so-called indistinguishability border α_{in} [58].

4. Conclusions

We summarize here the results on applications of uniaxial crystals for manipulating polarization states of light. We have shown that laser beams traveling in birefringent media can be thought of as the superposition of the radially and azimuthally polarized beams, for purely uniaxial crystal, and as the superposition of the spirally polarized beams in the birefringent chiral crystals. We have experimentally and theoretically revealed that uniaxial crystals are able to shape different beam types in mono- and polychromatic light. The circularly polarized beam components carry the optical vortices whose topological charges differs by two units. The control of the vortex

positions in the beam can be performed by means of a phase plate. The beam inclination relative to the crystal optical axis results in violating the axial symmetry of the field and the beams acquire new properties. In particular, we have experimentally and theoretically considered the formation of the single charged optical vortices and analyzed the phenomenon of the beam quadrefringence caused by the transverse shift of the center of gravity in one of the circularly polarized field component.

Acknowledgment

This work was supported by the Australian Research Council.